L-subshell fluorescence yields and Coster-Kronig transition probabilities with a reliable uncertainty budget for selected high- and medium-*Z* elements

Michael Kolbe, Philipp Hönicke, Matthias Müller, and Burkhard Beckhoff
Physikalisch-Technische Bundesanstalt (PTB), Abbestrasse 2-12, 10587 Berlin, Germany
(Received 31 May 2012; published 19 October 2012)

Photon-in/photon-out experiments at thin specimens have been carried out to determine *L*-subshell fluorescence yields as well as Coster-Kronig transition probabilities of Au, Pb, Mo, and Pd using radiometrically calibrated instrumentation in the Physikalisch-Technische Bundesanstalt (PTB) laboratory at the electron storage ring BESSY II in Berlin. An advanced approach was developed in order to derive the fluorescence line intensities by means of line sets of each subshell that were corrected for self-absorption and broadened with experimentally determined detector response functions. The respective photoelectric cross sections for each subshell were determined by means of transmission measurements of the same samples without any change in the experimental operating condition. All values derived were compared to those of earlier works. A completely traceable uncertainty budget is provided for the determined values.

DOI: 10.1103/PhysRevA.86.042512 PACS number(s): 32.30.Rj, 78.70.En, 32.50.+d

I. MOTIVATION

The complete understanding of atomic excitation and emission processes as well as the exact knowledge of related cross sections are crucial for quantitative investigations of elemental concentrations in unknown specimens by x-ray spectrometry. The emitted spectral response of an unknown sample following the excitation by x rays is based on both the specimen's elemental composition and the related atomic processes, the probability of which depends on a set of atomic fundamental parameters. For the quantitative determination of the respective elemental concentrations, the cross sections for photoionization of the (sub)shell and for both elastic and inelastic scattering, the related fluorescence yield, and transition probabilities associated with the specific inner-shell excitations have to be exactly known. Therefore, the uncertainty of these fundamental parameters is relevant for reference-based as well as reference-free x-ray fluorescence analysis results. Here, a reliable uncertainty budget is needed [1–3].

Krause *et al*. [4] estimated relative uncertainties by comparing of theoretical total photoionization cross sections with those determined experimentally, which have still mostly remained valid since the late 1970's [5]. In addition, one may assume that most of the relative uncertainties are estimated rather from the compilation of available data than from the individual experimental uncertainty budget. An example of a compilation-based uncertainty indication is the compilation of theoretical data by Puri *et al*. published in 1993 for elements $25 \leqslant Z \leqslant 96$ based on the relativistic Dirac-Hartree-Slater model [6], which states only a fitting error of 2% for elements with higher Z.

The fluorescence yields as well as Coster-Kronig (CK) transition probabilities were investigated in earlier works, e.g., by electron-induced high-resolution x-ray fluorescence spectroscopy, $K\alpha$-$L\alpha$-coincidence methods [7]. When monochromatic tunable synchrotron radiation became available, photoionization experiments were also carried out, but the respective relative uncertainties could not be reduced significantly [5]. This was partially caused by the unknown efficiency of uncalibrated instrumentation and insufficient knowledge of the detector response behavior.

Krause has performed numerical calculations for average *L*-shell fluorescence, Auger, and electron yields based on the evaluation of subshell radiative and radiationless yields [8]. Due to the strong correlation between fluorescence yields ω_i and Coster-Kronig transition probabilities $f_{i,k}$, the relative uncertainty for the average fluorescence yield determined was estimated to range between 2% and 5%. A comparison with experimental data available at that time showed an agreement between calculation and measurements [8] within the somewhat higher relative uncertainties of the experimentally deduced values.

In 1985 Jitschin *et al*. published photoionization measurements employing monochromatized synchrotron radiation for the determination of Coster-Kronig and fluorescence yields of Au *L* subshells [9]. For the first time, they reported on a direct derivation of the Coster-Kronig transition probabilities by recording the fluorescence radiation, when tuning the photon energy of the incident radiation across all three *L* absorption edges, a method which is also used in the current work. In contrast to the current work, different foils were used for the fluorescence measurements and the determination of the mass absorption coefficient for the derivation of the subshell photoionization cross sections, thus increasing the uncertainties related to the potentially different foil properties, such as the local homogeneity, pinhole density, impurities, and thicknesses. Jitschin *et al*. [9] have taken the energy dependence of the cross sections as predicted by theory [10–12]. Instead of absolute measurements of the photoionization cross sections, the data were normalized by setting the experimental $L3$ cross section equal to the theoretical value. Thus, deviations between experimental and theoretical data of up to 9% were found [9]. For the determination of Coster-Kronig transition probabilities, the intensity of only one single line of each subshell was evaluated, hence the knowledge of the transition probability of the selected fluorescence line is necessary and contributes to the uncertainty budget.

In a more recent paper Jitschin describes the progress in the measurements of L-subshell fluorescence, Coster-Kronig, and Auger yields in the 1980's [13]. At that time electron storage rings providing synchrotron radiation became important as tunable x-ray sources for the selective excitation of subshells and thus could further improve measurements of fundamental atomic parameters. The theoretically and experimentally determined values for the K-shell fluorescence yields could be determined with relative uncertainties of only a few percent. However, the situation for L-subshell yields remained quite different. The uncertainties are mainly affected by the uncertainties in the determination of ionization cross sections as well as fluorescence line intensities. The latter is especially caused by overlapping fluorescence lines and less well-known detection efficiencies. The direct determination of fluorescence yields by comparing the number of absorbed photons and emitted x-rays, which needs calibrated detectors for both the incident and the fluorescent radiation, had not yet been performed. Furthermore, the accuracy of synchrotron radiation-based methods depended on the knowledge of the subshell photoionization cross sections [13], which can be affected by considerable chemical binding state [x-ray absorption near edge structure (XANES)], solid-state [extended x-ray absorption fine structure (EXAFS)], and electron correlation effects.

For further reducing of the relative uncertainties the absolute calibration of the detectors to measure incident as well as fluorescent radiation is crucial and represents one of the main techniques used in the current paper. Furthermore, in the present work effective spectra deconvolution is performed by one set of the fluorescence lines belonging to each subshell, including their absorption-corrected relative intensities as well as experimentally determined subshell photoionization cross sections. This evaluation procedure is introduced here. Furthermore, the same sample was used in an identical beam geometry for both the absorption and the fluorescence measurements.

An overview of recently measured x-ray fluorescence cross sections and yields is given by Kacal *et al.* in Ref. [14].

II. THEORY

The fluorescence intensity is calculated according to Sherman's equation in the case of thin one-elemental foils by a product of the incoming photon intensity with a geometrical factor including the solid angle of detection and the detection efficiency, the self-absorption correction factor, and a fluorescence production factor. The latter is the product of the photoelectric cross section, the fluorescence yield, and includes the Coster-Kronig transition probabilities from case to case. The self-absorption correction factor considers the absorption of the incoming photons on their way to as well as of the fluorescence photons on their way from the place of photoionization in the sample, respectively. Using tunable photon sources, this factor can be easily determined experimentally by transmission measurements at the relevant photon energies.

For the definition of the Coster-Kronig transition probabilities the following description will be used (cf. Ref. [9]). Due to the possible transfer of initial vacancies from $L1$ and $L2$ subshells to higher L subshells, the cross sections σ for each subshell can be written as follows:

$$\begin{aligned}\sigma_{L1}(E_0) &= \omega_{L1}\tau_{L1}(E_0),\\ \sigma_{L2}(E_0) &= \omega_{L2}[\tau_{L2}(E_0) + \tau_{L1}(E_0) f_{1,2}],\\ \sigma_{L3}(E_0) &= \omega_{L3}[\tau_{L3}(E_0) + \tau_{L2}(E_0) f_{2,3}\\ &\quad + \tau_{L1}(E_0)(f_{1,3} + f_{1,2} f_{2,3})],\end{aligned} \tag{1}$$

where ω_{Li} is the fluorescence yield and τ_{Li} the photoelectric cross section of the subshell Li. $f_{i,j}$ are the Coster-Kronig transition probabilities. For photon energies below the respective subshell edge energy these values are not relevant. Therefore, it is possible by a specific selection of monochromatic excitation to avoid or to allow for additional contributions to the vacancy distribution of a specific subshell.

Using an energy below E_{L3}, all τ_{Li} are zero. For energies between E_{L3} and E_{L2} only τ_{L3} is unequal to zero. Therefore, in this energy region with a known photoelectric subshell cross section τ_{L3} the fluorescence yield ω_{L3} can be derived because the third line of Eq. (1) is $\sigma_{L3}(E_0) = \omega_{L3}\tau_{L3}(E_0)$ for $E_{L3} < E_0 < E_{L2}$. $\sigma_{L1}(E_0)$ and $\sigma_{L2}(E_0)$ are zero. By further increasing the energy above the $L2$ absorption edge, Eq. (1) changes to

$$\left.\begin{aligned}\sigma_{L1}(E_0) &= 0,\\ \sigma_{L2}(E_0) &= \omega_{L2}\tau_{L2}(E_0),\\ \sigma_{L3}(E_0) &= \omega_{L3}[\tau_{L3}(E_0) + \tau_{L2}(E_0) f_{2,3}],\end{aligned}\right\} \text{for}\quad E_{L2} < E_0 < E_{L1}. \tag{2}$$

Thus the fluorescence yield of subshell $L2$ and the Coster-Kronig yield $f_{2,3}$ are determinable in this energy region. In the energy region above the $L1$ edge the fluorescence yield of subshell $L1$ and the Coster-Kronig yield $f_{1,2}$ and $f_{1,3}$ can be resolved by knowing the yields determined at lower photon energies.

These equations demonstrate the importance of knowing the photoelectric cross section of each subshell for the determination of the fluorescence yields. Transmission measurements allow for the determination of these cross sections. The well-known Lambert-Beer law describes the relation between the linear mass absorption coefficient, the thickness, and the transmittance of the sample:

$$I_{\text{tr}}(E) = I_0(E)\exp[-\mu(E)\rho d]. \tag{3}$$

Knowing the density ρ and the thickness d of the sample, its mass attenuation coefficient μ, which is the sum of the coherent and incoherent scattering cross section as well as of the photoelectric cross section, can be obtained. The total photoelectric cross section is composed of the photoelectric cross section of the subshells. Determining the subshell cross section by multiplying the total photoelectric cross section with the jump ratio is often done, but leads to incorrect results as the contribution of the $L1$ relative to the $L2,3$ subshell cross sections varies with the distance from the corresponding edges due to their different energy dependencies.

III. EXPERIMENTS

For the fluorescence and transmission measurements, two different beamlines at the electron storage ring BESSY II in Berlin were used. The investigations of Au and Pb were

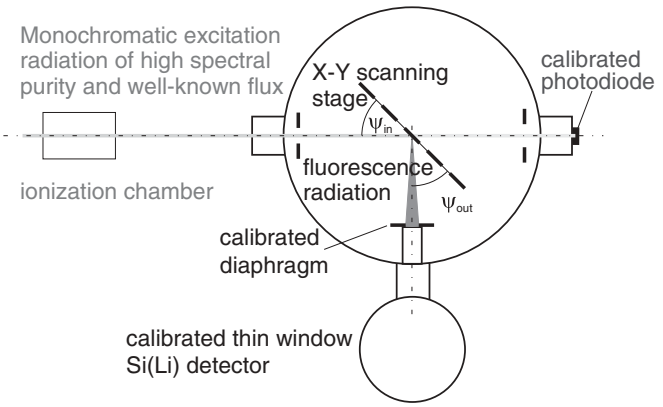

FIG. 1. Experimental setup showing the calibrated instrumentation employed in XRF beam geometry.

carried out at a 7-T wavelength shifter (WLS) beamline, the BAMline [15,16]. For the investigations of Pd and Mo, the incident radiation was provided by the four-crystal monochromator (FCM) beamline for bending magnet radiation in the Physikalisch-Technische Bundesanstalt laboratory at the electron storage ring BESSY II [17]. This beamline provides monochromatized radiation between 1.75 and 10.5 keV by means of either four InSb(111) or Si(111) crystals. For Pd and Mo, the incident photon energy was varied from below the $L3$ edge up to energies above the $L1$ edge using the Si crystals. The beam diameter in the focal plane, where the measurement chamber is placed, is about 250 μm.

For the experiments, an in-house developed ultrahigh vacuum chamber dedicated for reference-free x-ray fluorescence analysis was placed in the focal plane of the beamlines. Prior to the samples an ionization chamber (BAMline) or a thin transmission diode (FCM), respectively, were used for monitoring purposes. As there was no direct connection to the BAMline, the monochromatized beam from this beamline entered the vacuum chamber through a 75-μm-thick beryllium window. The relative intensities of higher harmonics at the BAMline were determined by a calibrated high-purity germanium detector [16] and are below 2×10^{-5}. At the FCM, the contributions are even lower in the spectral range employed for the current measurements [17]. Thus the contribution from higher harmonics has only a negligible influence on the uncertainty budget of the measurement.

In the center of this chamber an X-Y scanning stage for sample positioning was arranged in a 45°-45° geometry, thus ensuring a conventional x-ray fluorescence (XRF) geometry as shown in Fig. 1. Behind the sample holder a calibrated photodiode was placed for transmission measurements as well as for the determination of the incident radiant power during the XRF analysis or fundamental parameter (FP) determination. For this purpose, the relation between the calibrated photodiode in the chamber and the monitor signal in front of it was determined before and after each fluorescence measurement. The incident radiant power can be deduced by correlation with the monitor signal during the fluorescence measurement. The calibration of the photodiode is based on measurements with a cryogenic electrical substitution radiometer providing the efficiency of the diode with relative uncertainties below 1% [17]. The fluorescence radiation emitted by the sample was detected by calibrated energy dispersive detectors [Lithium-Drifted Silicon Detector (Si(Li)) at the BAMline or Silicon Drift Detector (SDD) at the FCM], which were placed behind a calibrated diaphragm at a well-defined distance from the sample. The diameter of the diaphragm is microscopically determined and defines the solid angle of detection with a relative uncertainty of 0.7% [18]. The radiometric calibration with regard to its detection efficiency and detector response function of such an energy dispersive detector is described in Refs. [19,20]. According to those references, the efficiency with a relative uncertainty of 1.5% in the region of interest here, as well as the detector response functions, are well known and the intensity of the fluorescence lines of the sample can be determined very accurately. Due to the full width at half maximum (FWHM) value of the detector response, which is about 180 eV for the energies of relevance here, the natural Lorentzian broadening of the fluorescence lines could be neglected.

Besides the diagram lines, satellite lines also appear in the spectrum [21,22]. These satellites are in the vicinity of their diagram lines and cannot be distinguished by our setup due to the limited energy resolution of the energy-dispersive x-ray detector. These satellite lines contribute to the fluorescence intensity of the diagram line. Due to their small difference in energy they are fitted together with the diagram lines.

The free-standing one-elemental foils of Au and Pb used for the investigation were manufactured by the Lebow Company with a nominal thickness of about 2 μm. Multiple photon energies (e.g., for Au: 12.019, 12.419, 13.684, 13.834, 14.034, 14.234, 14.455, 14.66, 15.0, 18.0; and for Pb: 13.8, 14.9, 15.35, 15.6, 16.5, 17.0, 18.0 keV) were chosen for the excitation of the heavy-element foils.

In order to determine the CK and fluorescence yields for Mo and Pd, thin-metal depositions with 250 nm thickness on 500 nm silicon nitride membranes were provided by AXO Dresden GmbH. The membranes were fabricated by means of a backside etch process of a silicon wafer piece with deposited Si_xN_y to create a free-standing membrane with a silicon frame. The metal layers were deposited onto the membranes using magnetron sputtering.

Besides the investigations at excitation energies, transmission measurements at the photon energies of the fluorescence lines were carried out in order to experimentally determine the absorption correction factor. Thus the knowledge of the absorption is independent of databases for the mass attenuation coefficient [23,24].

By applying

$$\sigma_{i,\mathrm{shell}}(E_0) = \omega_{i,\mathrm{shell}}\tau_{i,\mathrm{shell}}(E_0) = \frac{\Phi^d_{i,\mathrm{line}}(E_0)}{\Phi_0(E_0)\frac{\Omega}{4\pi}M_{X,i}} \qquad (4)$$

with the solid angle of detection $\frac{\Omega}{4\pi}$, the incident photon flux $\Phi_0(E_0)$, the fluorescent photon flux $\Phi^d_{i,\mathrm{line}}(E_0)$, and the absorption correction factor

$$M_{Xi} = \frac{\rho d}{\left(\frac{\mu_{s,E_0}}{\sin\psi_{\mathrm{in}}} + \frac{\mu_{s,E_f}}{\sin\psi_{\mathrm{out}}}\right)\rho d} \times \left\{1 - \exp\left[-\left(\frac{\mu_{s,E_0}}{\sin\psi_{\mathrm{in}}} + \frac{\mu_{s,E_f}}{\sin\psi_{\mathrm{out}}}\right)\rho d\right]\right\}, \qquad (5)$$

the yield of each subshell was determined according to Eq. (1).

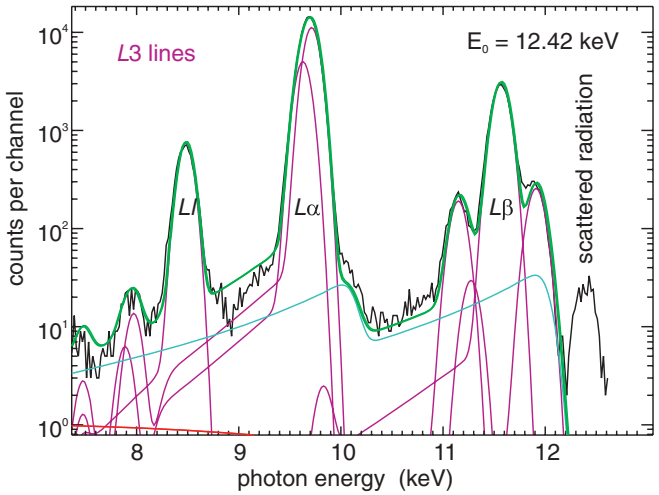

FIG. 2. (Color online) Determination of $L3$ fluorescence line set from the spectrum of Au recorded at an incident photon energy of 12.42 keV. As background contributions, bremsstrahlung as well as resonant Raman scattering at the $L2$ edge (with respect to the $M4$ and $N4/5$ shells) were considered. In the left part of the figure the escape lines of the detector response can be seen. In the background of the diagram lines, satellite lines are obviously present, the relative contribution of which can be estimated to be about or less than 1%. At 7.48 keV a low Ni $K\alpha$ line is visible, which is due to the nickel front contact of the detector part of its response function.

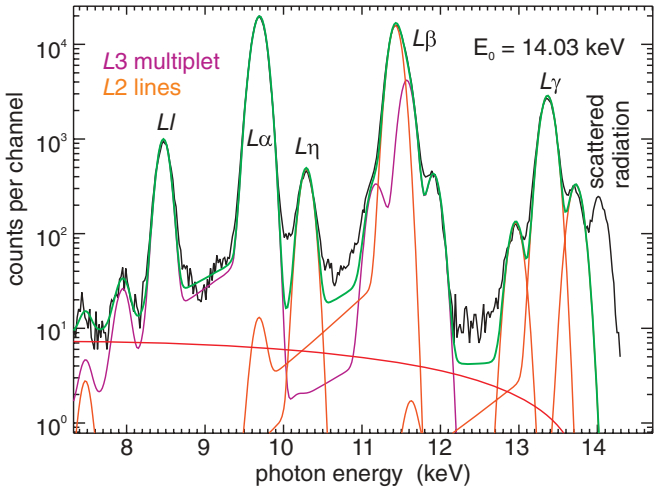

FIG. 3. (Color online) Determination of the $L2$ fluorescence line sets from the spectrum of Au recorded at an incident photon energy of 14.03 keV employing the $L3$ fluorescence lines set determined at energies below the $L2$ absorption edge with bremsstrahlung background contribution. The contribution of resonant Raman scattering at the $L1$ absorption edge in comparison with the bremsstrahlung is very low and not visible in this spectrum. At 7.48 keV a low Ni $K\alpha$ line is visible, which is due to the nickel front contact of the detector part of its response function.

IV. APPROACH AND TECHNIQUE

A. Determination of fluorescence intensities

The spectra recorded at different incident photon energies were evaluated as follows. Starting with an energy between the $L3$ and $L2$ edge, only the fluorescence lines belonging to the $L3$ subshell are excited. The energies of these lines, which may overlap with others, were determined with the help of several databases [24,25]. The accurate determination of the fluorescence line intensities is essential for FP determinations. Therefore the response functions of the detectors used were experimentally determined and theoretically modeled beforehand [19,20,26]. By convoluting a background contribution as described in Ref. [27] and each individual fluorescence line with the detector response function, a theoretical spectrum was fitted to the experimentally recorded one. Figure 2 shows the fit to the spectrum of a gold sample recorded at an excitation energy of 12.419 keV. Transition probabilities from the databases were not taken as preset values, thus allowing for an independent determination of the intensity of each line. Therefore, the influence of any potential uncertainties originating from the databases could be reduced. This strategy allows for an independent determination of the transition probabilities of lines sufficiently separated by the energy resolution of the detector, whereas the self-absorption and the detector efficiency are treated carefully. This kind of fitting procedure was repeated for all spectra with incident energies between the $L3$ and $L2$ absorption edges. Due to the change of the incident photon energy (from 12 to 18 keV), the self-absorption effects in the sample change slightly (about 10% for $M_{X,i}$). By means of experimental absorption correction factors $M_{X,i}$, which were determined from transmission measurements of the same sample at the exciting as well as at the respective fluorescence energies, relative intensities for the fluorescence lines of the $L3$ subshell could be determined. These transition probabilities, i.e., the relative line intensities corrected for absorption, have been evaluated and set as invariant constants in the following. The evolution of satellite lines for fluorescence lines belonging to the $L3$ subshell while increasing the excitation energy above the subsequent L edges has no significant influence. Due to their energy shift, which is below the resolution of the detector, they are fitted together with their diagram lines. To fix the relative line intensities of one subshell, the intensity of the satellite lines has to be added to that of the diagram lines as Müller *et al.* showed this exemplarily for nickel [28].

At photon energies between the $L2$ and $L1$ absorption edges, the absorption correction factor for each incident photon energy and fluorescence line of $L3$ was determined from the transmission measurements, the whole set of $L3$ lines was convoluted with the detector response function, and its experimentally determined relative intensities were fitted to the spectrum (see Fig. 3). For the fluorescence lines of the $L2$ subshell, the same procedure as before for the fluorescence lines of the $L3$ subshell was carried out. This means that the energy of each single fluorescence line was determined and convoluted with the detector response function. The $L3$ fluorescence line set was fitted together with all these single $L2$ fluorescence lines to the measured spectrum. Exactly the same procedure was performed for each incident photon energy between the $L2$ and $L1$ absorption edges. Thus relative intensities for each fluorescence line belonging to the $L2$ subshells were determined. The transition probabilities

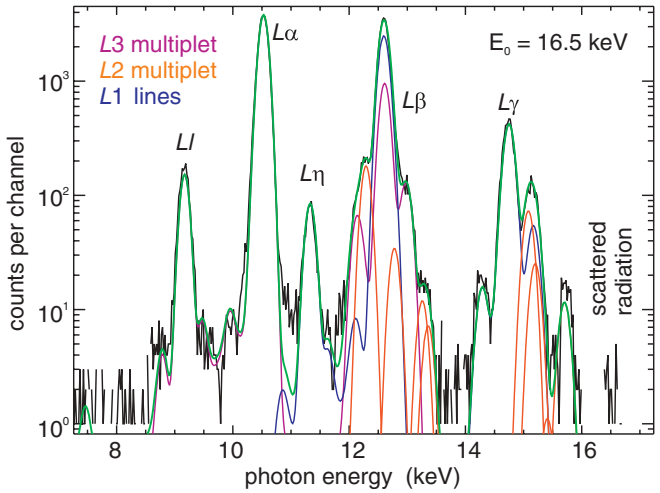

FIG. 4. (Color online) Determination of the $L1$ fluorescence line intensities from the spectrum of Pb recorded at an incident photon energy of 16.5 keV employing the $L3$ fluorescence lines set determined at energies below the $L2$ absorption edge and the $L2$ fluorescence lines set determined at energies below the $L1$ absorption edge.

of these lines were determined by the same procedure as performed before for the lines of the $L3$ subshell. By using the experimentally deduced absorption correction factors for each exciting and fluorescence energy for the fluorescence lines of the $L2$ subshell, an invariant line set for further investigation was derived.

In the case of photon energies above the $L1$ absorption edge, the set of $L3$ lines with its relative intensities corrected for absorption and the set of $L2$ lines likewise treated were fitted together with the single $L1$ line energies convoluted with the detector response function. Figures 4 and 5 show these fits above the respective $L1$ absorption edge exemplarily for Pb and Pd.

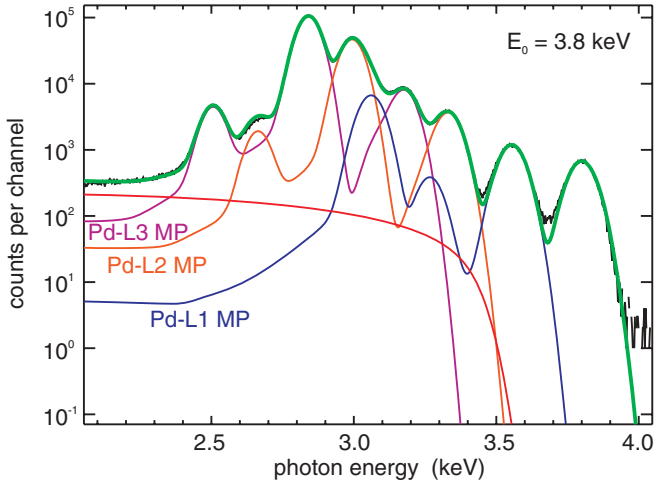

FIG. 5. (Color online) Spectrum of Pd recorded at an incident photon energy of 3.8 keV (above the $L1$ absorption edge) and its fit employing the multiplets (MP) of fluorescence lines set for each of the three L subshells and a bremsstrahlung background contribution.

This procedure results in a numerically very stable fitting behavior over this energy region and allowed for the determination of the fluorescence intensities of the lines belonging to each L subshell. Furthermore, the spectra deconvolution based on all these three line sets allows for the reduction of the uncertainties related to the determination of the fluorescence intensities from about 2.5% [18] to 1.5%.

In order to determine the fluorescence yields and Coster-Kronig transition probabilities by solving Eq. (1), the intensities of all lines belonging to one subshell were summed up. Being independent of the knowledge of transition probabilities for single lines allows for the reduction of the overall uncertainty. In contrast, the use of single lines such as Ll, which are less affected by overlapping fluorescence lines, would increase the uncertainty by involving the uncertainty of the knowledge of its specific transition probability. As the sum of the transition probabilities of all lines belonging to one subshell is equal to unity, the addition of the line intensities corrected for the absorption excludes potential further uncertainties associated with the values of the transition probabilities. However, the above procedure for the treatment of single lines of each line set ensures an optimal fitting behavior, and therefore the most reliable total intensities of the fluorescence radiation associated with each subshell can be obtained.

B. Determination of subshell photoelectric cross sections

As mentioned above, the knowledge of subshell photoelectric cross sections is crucial for the determination of the fluorescence yields and Coster-Kronig transition probabilities. Transmission measurements allow for the determination of the mass absorption coefficient, which includes the cross sections for coherent and incoherent scattering as well as photoelectric absorption. By investigating the transmission of the same sample, which was also used for the fluorescence analysis, two objectives were pursued.

On the one hand, the transmission measurements were carried out at the exciting as well as fluorescence line energies for the experimental determination of the mass absorption correction factor as it was used in the previous sections. On the other hand, these measurements were also used for the determination of subshell photoelectric cross sections. Converting Eq. (3), the energy dependence of the mass absorption coefficient $\mu(E)\rho d = -\ln(\frac{I_{tr}(E)}{I_0(E)})$ can be easily determined from transmission measurements. For the absolute determination of the mass absorption coefficient the accurate knowledge of the energy independent product of sample density and thickness (ρd) is necessary, gained e.g., by gravimetric measurements combined with the investigation of homogeneity. If the mass absorption coefficient is known at least for one specific energy, ρd can be determined for the sample. This would have the advantage of excluding any inhomogeneity or beam size and footprint effects. For higher photon energies, the tabulated mass absorption coefficients could be deduced more accurately from thicker foils, of which the thickness could be determined by a reliable independent method. For the determination of the subshell fluorescence yield as well as Coster-Kronig transition probabilities the absolute knowledge of ρd is not necessary as τ in Eq. (4)

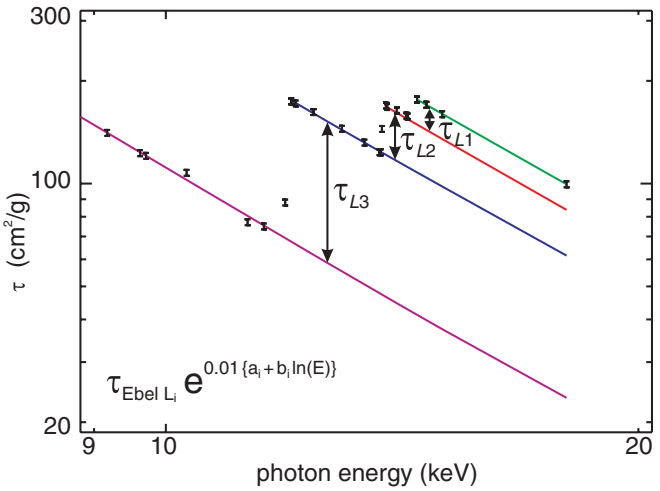

FIG. 6. (Color online) Determination of the energy dependence of the L-subshell photoelectric cross sections τ of Au from transmittance measurements modifying the respective cross sections of the Ebel database ($a_3 = -5.71$, $b_3 = -1.59$, $a_2 = 1.11$, $b_2 = -5.00$, $a_1 = 8.54$, $b_1 = -3.17$). The relative contributions of elastic and inelastic scattering (4.0×10^{-2} and 4.0×10^{-4} at 10 keV and 2.5×10^{-2} and 6.5×10^{-4} at 18 keV, respectively) to the total mass absorption coefficient were included in the transmittance evaluation based on the ratio of their theoretical values to the value of the photoelectric effect.

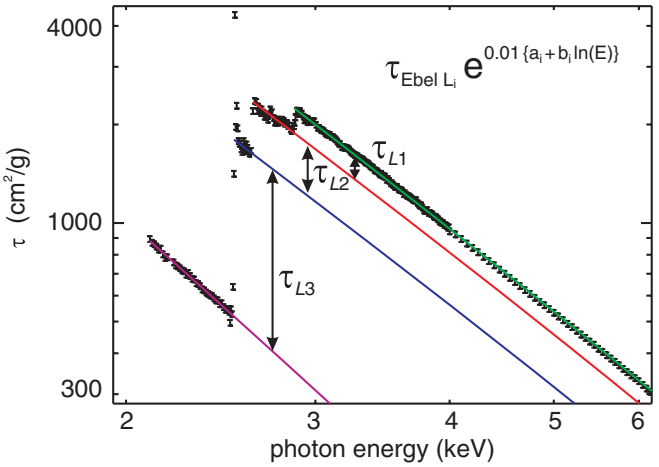

FIG. 7. (Color online) Determination of the energy dependence of the L-subshell photoelectric cross sections τ of Mo from transmittance measurements modifying the respective cross sections of the Ebel database ($a_3 = -8.2$, $b_3 = 0$, $a_2 = -3.8$, $b_2 = 0$, $a_1 = 2.5$, $b_1 = -2.2$). The relative contributions of elastic and inelastic scattering (1.0×10^{-2} and 3.7×10^{-5} at 2.5 keV and 4.7×10^{-3} and 3.4×10^{-5} at 4 keV, respectively) to the total mass absorption coefficient were included in the transmittance evaluation based on the ratio of their theoretical values to the one of the photoelectric effect.

will be multiplied by ρd, allowing for the determination of $\frac{M_{Xi}}{\rho d}$ just by transmission measurements [2].

Recently a database of mass attenuation and photoelectric cross sections has been compiled by Ebel *et al.* [23]. Based on the calculations of Scofield, available data of different databases were analyzed and compared with empirical data. By introducing least-squares fits of fifth order polynomials to the best values, numerical data were composed in a database, developed especially for applications in fundamental parameter algorithms for quantitative x-ray fluorescence analysis. The experimentally determined data for the mass absorption coefficient were partitioned in line with their relative database values into their scattering and photoelectric cross sections, thus external knowledge on cross-section ratios, but not on the respective absolute values, has to be employed. Therefore, the photoelectric cross section needed for the evaluation of the fluorescence measurements could be separated from the only slightly varying scattering cross section by using their ratio as given in the database [23] according to $\tau\rho d = \mu_{\text{expt}}\rho d\frac{\tau_{\text{DB}}}{\mu_{\text{DB}}} = \mu_{\text{expt}}\rho d(1 - \frac{\sigma_{\text{cohDB}}+\sigma_{\text{incohDB}}}{\mu_{\text{DB}}})$. By employing this procedure the knowledge of the absolute value of ρd is not necessary and accordingly has no impact on the uncertainty budget.

The determination of the photoelectric cross section of each subshell is based on the comparison of the experimental data to the database as well. The run of the subshell photoelectric cross sections was adopted from the Ebel database by slightly changing the polynomial coefficients of the first and second order to fit the theoretical data to the experimentally deduced ones as shown for Au in Fig. 6 and for Mo in Fig. 7. Therefore, an adopted experimentally determined photoelectric cross section for each subshell at different incident energies could be derived and used further on for the determination of Coster-Kronig transition probabilities and fluorescence yields.

The uncertainty for the deduced subshell cross sections has to include the experimental uncertainty of the transmission measurement, which depends, e.g., on the sample homogeneity and its pinholes, the invariant beam spot size, the linearity, and the dark current of the photodiode used during the measurements, as well as on the uncertainties of the database values. Assuming for the database-related scattering cross sections σ_{cohDB} and σ_{incohDB} relative uncertainties of 0.1 and

TABLE I. Fluorescence yields and Coster-Kronig transition probabilities of Au derived in the present work as compared to corresponding values achieved earlier by other authors.

	Present work	Jitschin [9]	Krause [29]	Puri [6]	Chen [30] (interpolated)	Cullen [31]
$\omega_{L3,\text{Au}}$	0.310 ± 0.011	0.320 ± 0.010	0.320 ± 0.010	0.313	0.312	0.318
$\omega_{L2,\text{Au}}$	0.359 ± 0.013	0.401 ± 0.020	0.334 ± 0.017	0.358	0.354	0.363
$\omega_{L1,\text{Au}}$	0.117 ± 0.004	0.135 ± 0.009	0.107 ± 0.016	0.078	0.077	0.082
$f_{\text{CK12,Au}}$	0.064 ± 0.040	0.047 ± 0.010	0.14 ± 0.02	0.068	0.071	0.07
$f_{\text{CK13,Au}}$	0.524 ± 0.075	0.590 ± 0.020	0.53 ± 0.03	0.711	0.711	0.701
$f_{\text{CK23,Au}}$	0.180 ± 0.040	0.100 ± 0.009	0.122 ± 0.018	0.129	0.129	0.128

TABLE II. Fluorescence yields and Coster-Kronig transition probabilities of Pb derived in the present work as compared to corresponding values achieved earlier by other authors.

	Present work	Krause [29]	Puri [6]	Chen [30] (interpolated)	Cullen [31]
$\omega_{L3,\mathrm{Pb}}$	0.369 ± 0.013	0.360 ± 0.011	0.343	0.342	0.352
$\omega_{L2,\mathrm{Pb}}$	0.513 ± 0.018	0.373 ± 0.019	0.397	0.392	0.404
$\omega_{L1,\mathrm{Pb}}$	0.134 ± 0.005	0.112 ± 0.017	0.093	0.093	0.098
$f_{\mathrm{CK12,Pb}}$	0.010 ± 0.009	0.12 ± 0.02	0.054	0.061	0.056
$f_{\mathrm{CK13,Pb}}$	0.664 ± 0.100	0.58 ± 0.03	0.708	0.699	0.698
$f_{\mathrm{CK23,Pb}}$	0.141 ± 0.040	0.116 ± 0.017	0.123	0.124	0.122

for the corresponding photoelectric cross sections τ_{DB} an uncertainty of 0.02 error propagation reveals a total relative uncertainty of the experimentally derived cross sections τ of about 2%. Due to reliable transmission measurements without solid-state effects between the respective absorption edges for high-Z elements, this uncertainty value does not increase for the subshell cross sections τ_{Li}, whereas for the medium-Z elements increased uncertainties have to be considered. For the photoelectric subshell cross section τ_{L2} the uncertainty of τ_{L3} has to be included and for τ_{L1} the uncertainties determined for τ_{L3} as well as τ_{L2}, resulting in uncertainties of 4% and 7%, respectively, for Mo and Pd.

V. RESULTS AND DISCUSSION

By employing the described techniques and using Eqs. (1) and (2) the subshell fluorescence yields as well as the various Coster-Kronig transition probabilities were determined. Tables I–IV show the results obtained by this approach for the investigated samples in comparison to values published earlier by other authors. For the fluorescence yield ω_{L3} and the Coster-Kronig transition probability f_{CK13} the values in dependence on the atomic number are shown in Figs. 8 and 9.

The relative uncertainty associated with the fluorescence yields is about 3.5% based on the relative uncertainties given in the experimental part of this paper and Eq. (3). Apart from the contributions associated with the detector efficiencies and the solid angle of detection, the total relative uncertainty is mainly affected by the contribution from the counting statistics and the spectra deconvolution procedure.

The estimates of the uncertainties given by Krause [29] are based on stated and presumed reliabilities of the material used for the data compilation. Apart from this, the degree of compatibility of different relevant data was a basis for the estimation of the uncertainties assigned to the adopted values for the fluorescence yields as well as the Coster-Kronig transition probabilities. The estimated relative uncertainties range from 3% for the fluorescence yield of the $L3$ subshell up to 20% for the Coster-Kronig transition probability $f_{\mathrm{CK12_{Au}}}$, whereas it is stated that this uncertainty may be enlarged due to a stronger variance of the Coster-Kronig factor in dependence on the atomic number.

Jitschin *et al.* [9] normalized their data to the fluorescence yield for the $L3$ subshell given by Krause [29], which was considered to be the most reliable value. The uncertainties for the other values given include those for the determination of the subshell cross sections as well as of the intensities of characteristic lines, where the ratios for weaker lines were included by calculated values taken from theory. Furthermore, statistical uncertainties were included and systematic effects were estimated. The determination of the uncertainties of the Coster-Kronig factors of Jitschin *et al.* [9] could not be comprehended. As clearly stated, these factors depend on the relation between the cross sections belonging to the subshells. For the photoionization cross sections the relative uncertainties range from only a few percent up to 5%. Hence, the relation between these values should have at least relative uncertainties in the same order. In view of error propagation, a relative uncertainty of 3% stated for $f_{\mathrm{CK13_{Au}}}$ appears to be rather small.

The uncertainties given for the values of Puri *et al.* [6] are only the fitting errors (2%) of the least-squares fit as a function of the atomic number. The comparison of these uncertainties with experimentally determined values seems to be inadequate and is not explicitly stated in the tables.

The relative uncertainties of the Coster-Kronig factors in the present work are higher than those of the fluorescence yields because of the performed error propagation based on the relation between the different subshell cross sections. The absolute uncertainty of large values such as the subshell cross sections with a relative uncertainty of about 3%–4% increases the relative uncertainty for a small value rather strongly, i.e., the Coster-Kronig factor, deduced as a difference of two

TABLE III. Fluorescence yields and Coster-Kronig transition probabilities of Pd derived in the present work as compared to corresponding values achieved earlier by other authors.

	Present work	Krause [29]	Puri [6]	Chen [30] (interpolated)	Cullen [31]	Cao [32]
$\omega_{L3,\mathrm{Pd}}$	0.050 ± 0.002	0.049 ± 0.01	0.052	0.055	0.053	
$\omega_{L2,\mathrm{Pd}}$	0.046 ± 0.002	0.047 ± 0.01	0.05	0.053	0.051	
$\omega_{L1,\mathrm{Pd}}$	0.015 ± 0.001	0.014 ± 0.004	0.01	0.01	0.012	
$f_{\mathrm{CK12,Pd}}$	0.08 ± 0.08	0.100 ± 0.02	0.065	0.058	0.075	0.047 ± 0.01
$f_{\mathrm{CK13,Pd}}$	0.589 ± 0.131	0.600 ± 0.06	0.750	0.751	0.723	0.730 ± 0.039
$f_{\mathrm{CK23,Pd}}$	0.129 ± 0.044	0.151 ± 0.03	0.154	0.153	0.156	0.164 ± 0.033

TABLE IV. Fluorescence yields and Coster-Kronig transition probabilities of Mo derived in the present work as compared to corresponding values achieved earlier by other authors.

	Present work	Krause [29]	Puri [6]	Chen [30] (interpolated)	Cullen [31]
$\omega_{L3,\mathrm{Mo}}$	0.032 ± 0.001	0.037 ± 0.007	0.038	0.04	0.038
$\omega_{L2,\mathrm{Mo}}$	0.032 ± 0.001	0.034 ± 0.009	0.036	0.038	0.037
$\omega_{L1,\mathrm{Mo}}$	0.009 ± 0.001	0.01 ± 0.003	0.007	0.007	0.007
$f_{\mathrm{CK12,Mo}}$	0.182 ± 0.096	0.10 ± 0.02	0.056	0.067	0.063
$f_{\mathrm{CK13,Mo}}$	0.57 ± 0.14	0.610 ± 0.061	0.771	0.737	0.763
$f_{\mathrm{CK23,Mo}}$	0.203 ± 0.039	0.141 ± 0.0282	0.132	0.136	0.134

rather large values. Hence, a reliable uncertainty budget for the determined Coster-Kronig factors leads to uncertainties of 15%–30%, and for f_{CK12} even in the order of the value itself.

Here, a compilation of fluorescence as well as Coster-Kronig yields for the L subshells is given with comprehensible uncertainties, whereas estimated uncertainties had to be used only for the partition of the determined mass absorption cross section into the photoelectric as well as the coherent and incoherent scattering cross sections.

In view of the linear polarization of the synchrotron radiation in the plane of the storage ring, and, therefore, in the experimental plane defined by the direction of the incident as well as fluorescent radiation, some remarks on its potential influence on the angular distribution of fluorescence radiation are to be added here. Due to this 45°-45° arrangement, scattered incident radiation in direction of the Si(Li) or SDD detector could be reduced to a minimum. Thus, the scattered radiation, which would appear in the vicinity of the fluorescence lines due to the chosen excitation energies, only slightly affects the spectra deconvolution.

Furthermore, polarization effects are supposed to only slightly influence the angular distribution of the fluorescence radiation of L subshells. This effect has been studied earlier. Recently Santra *et al.* [33] published experimental results for Au employing 22.6-keV photons from a ^{109}Cd source. They reported a maximum anisotropy of 5% of the $L\alpha$ line with an instrumentation having a relative uncertainty of already 2% in the case of an isotropic emission characteristic. However, Yamaoka *et al.* had also studied the angular distribution of Au L fluorescence lines following photoionization by monochromatized synchrotron radiation with energies in the vicinity of the L subshells [34,35]. They had found that in the case of the Au Ll fluorescence line an anisotropy of just a few percent might be possible, whereas the expected anisotropy of the $L\alpha$ lines should be at least one order of magnitude lower, thus being somewhere in the per mille range which is not in line with some of the later findings [33] despite the undisputable fact that both works are based on the same theoretical considerations of Berezhko *et al.* [36]. Due to their experimental uncertainties Yamaoka *et al.* were not able to exclude the possibility of a weak angular dependence for this fluorescence line [35]. Yamaoka *et al.* also studied more recently the influence of Coster-Kronig transitions on such a possible anisotropy [37]. Their results show only a small effect of Coster-Kronig transitions on the anisotropy of the Au Ll fluorescence line, the line studied in this investigation.

Due to this conclusion, the present work, which relies mostly on the set of diagram lines of each subshell, does not take into account such an angular distribution as it is insignificant for the determination of the fluorescence yields as well as Coster-Kronig transition probabilities in view of the other more relevant contributions to the uncertainty budget as stated above.

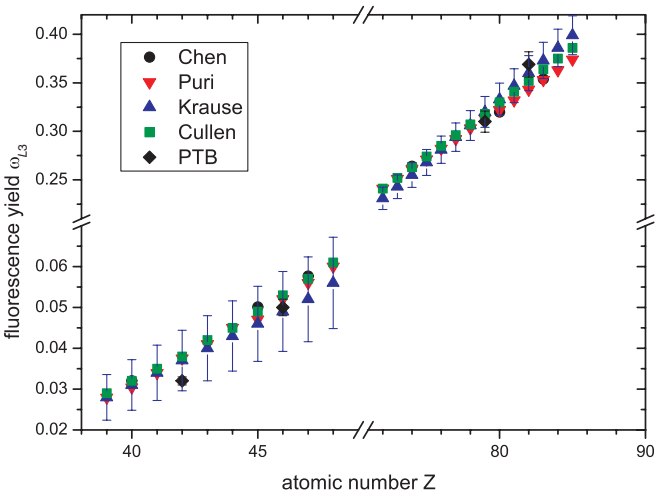

FIG. 8. (Color online) Comparison of the fluorescence yield $\omega_{L\mathrm{III}}$ in dependence on the atomic number as published by different authors.

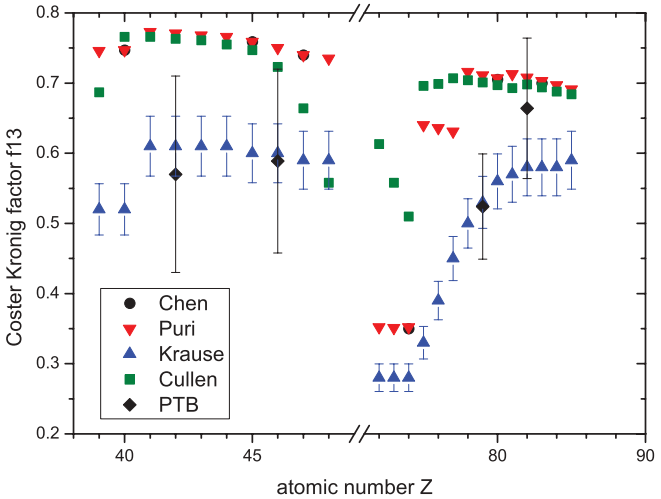

FIG. 9. (Color online) Comparison of the Coster-Kronig factor f13 in dependence on the atomic number as published by different authors.

VI. CONCLUSION AND PERSPECTIVES

Employing radiometrically calibrated equipment and advanced evaluation techniques, fluorescence yields as well as Coster-Kronig transition probabilities of the *L* subshells of Mo, Pd, Au, and Pb have been determined with a reliable uncertainty budget. The main advantage of the technique described in this paper is the total independence of any absolute value of the tabulated fundamental parameter. Uncertainties induced by changes in the experimental setup could be substantially decreased due to the determination of the photoelectric cross section as well as the yields and the mass absorption correction factor using the same sample in the same beam geometry.

Applying the introduced multiplet-fitting procedure results in a numerically very stable fitting behavior and allowed for the determination of the fluorescence intensity of the emission lines belonging to each *L* subshell even if the energy resolution of the detector is not sufficient for the separation of the single lines. The introduced multiplet-fitting procedure of spectra deconvolution makes the explicit reduction of the uncertainties for the determination of the fluorescence intensities possible, and therefore, in addition to the improved atomic fundamental parameters, for more reliable results in quantitative x-ray fluorescence analysis.

ACKNOWLEDGMENTS

The authors would like to thank F. Reinhardt and J. Weser (both PTB) as well as H. Riesemeier and E. Strub from the Federal Institute for Materials Research and Testing (BAM) for support in carrying out the experiments and for fruitful discussions. The financial support of this research within the framework of the EFRE/*Pro*FIT program funded project "Quantitation in x-ray fluorescence analysis" by the Investitionsbank Berlin as well as by the MNPQ-Transfer program of the German Federal Ministry of Economics and Technology is gratefully acknowledged.

[1] J. Sherman, ASTM Spec. Tech. Publ. I **57**, 27 (1954).
[2] B. Beckhoff and G. Ulm, Adv. X-Ray Anal. **44**, 349 (2001).
[3] B. Beckhoff, J. Anal. At. Spectrosc. **23**, 845 (2008).
[4] M. O. Krause, C. W. Nestor, Jr., C. J. Sparks, Jr., and E. Ricci, Oak Ridge National Laboratory Report No. ORNL-5399, 1978 (unpublished).
[5] G. Zschornack, *Handbook of X-Ray Data* (Springer, Berlin, 2007).
[6] S. Puri, D. Metha, B. Chand, N. Singh, and P. N. Trehan, X-Ray Spectrom. **22**, 358 (1993).
[7] W. Jitschin, in *Proceedings of the 15th International Conference on X-Ray and Inner-Shell Processes*, edited by T. A. Carlson, S. T. Manson, and M. O. Krause, AIP Conf. Proc. No. 215 (AIP, Melville, NY, 1990), p. 408.
[8] M. O. Krause, Phys. Rev. A **22**, 1958 (1980).
[9] W. Jitschin, G. Materlik, U. Werner, and P. Funke, J. Phys. B: At. Mol. Phys. **18**, 1139 (1985).
[10] J. H. Scofield, Lawrence Livermore Laboratory Report No. UCRL-51326, 1973 (unpublished).
[11] W. J. Veigele, At. Data Tables **5**, 51 (1973).
[12] J. A. Bearden, Rev. Mod. Phys. **39**, 78 (1967).
[13] W. Jitschin, U. Werner, G. Materlik, and G. D. Doolen, Phys. Rev. A **35**, 5038 (1987).
[14] M. R. Kacal, I. Han, F. Akman, and R. Durak, J. Quant. Spectrosc. Radiat. Transfer **113**, 373 (2012).
[15] W. Görner, M. P. Hentschel, B. R. Müller, H. Riesemeier, M. Krumrey, G. Ulm, W. Diete, U. Klein, and R. Frahm, Nucl. Instrum. Methods Phys. Res., Sect. A **467-468**, 703 (2001).
[16] H. Riesemeier, K. Ecker, W. Görner, B. R. Müller, M. Radtke, and M. Krumrey, X-Ray Spectrom. **34**, 160 (2005).
[17] M. Krumrey and G. Ulm, Nucl. Instrum. Methods Phys. Res., Sect. A **467-468**, 1175 (2001).
[18] M. Kolbe, B. Beckhoff, M. Krumrey, and G. Ulm, Spectrochim. Acta, Part B **60**, 505 (2005).
[19] F. Scholze and M. Procop, X-Ray Spectrom. **30**, 69 (2001).
[20] M. Krumrey, M. Gerlach, F. Scholze, and G. Ulm, Nucl. Instrum. Methods Phys. Res., Sect. A **568**, 364 (2006).
[21] H. Oohashi, Y. Ito, T. Tochio, A. M. Vlaicu, and T. Mukoyama, Phys. Rev. A **73**, 022507 (2006).
[22] H. Oohashi, Y. Ito, T. Tochio, A. M. Vlaicu, H. Yoshikawa, and S. Fukushima, Phys. Scr. **75**, 323 (2007).
[23] H. Ebel, R. Svagera, M. F. Ebel, A. Shaltout, and J. H. Hubbell, X-Ray Spectrom. **32**, 442 (2003).
[24] W. T. Elam, B. D. Ravel, and J. R. Sieber, Radiat. Phys. Chem. **63**, 121 (2002).
[25] NIST online database http://physics.nist.gov/PhysRefData/XrayTrans.
[26] F. Scholze, B. Beckhoff, M. Kolbe, M. Krumrey, M. Müller, and G. Ulm, Microchim. Acta **155**, 275 (2006).
[27] M. Müller, B. Beckhoff, G. Ulm, and B. Kanngießer, Phys. Rev. A **74**, 012702 (2006).
[28] M. Müller, B. Beckhoff, R. Fliegauf, and B. Kanngießer, Phys. Rev. A **79**, 032503 (2009).
[29] M. O. Krause, J. Phys. Chem. Ref. Data **8**, 307 (1979).
[30] M. H. Chen, B. Crasemann, and H. Mark, Phys. Rev. A **24**, 177 (1981).
[31] D. E. Cullen, J. H. Hubbell, and L. Kissel, EPDL97: The Evaluated Photon Data Library, '97 Version, Lawrence Livermore National Laboratory report, UCRL-50400, Vol. 6, Rev. 5, September 1997.
[32] W. Cao, J. Hoszowska, J.-Cl. Dousse, Y. Kayser, M. Kavcic, M. Zitnik, K. Bucar, A. Mihelic, J. Szlachetko, and K. Słabkowska, Phys. Rev. A **80**, 012512 (2009).
[33] S. Santra, D. Mitra, M. Sarkar, and D. Bhattacharya, Phys. Rev. A **75**, 022901 (2007).
[34] H. Yamaoka, M. Oura, K. Takahiro, T. Morikawa, S. Ito, M. Mizumaki, S. Semenov, N. Cherepkov, N. Kabachnik, and T. Mukoyama, J. Phys. B: At. Mol. Opt. Phys. **36**, 3889 (2003).
[35] H. Yamaoka, M. Oura, K. Takahiro, N. Takeshima, K. Kawatsura, M. Mizumaki, U. Kleiman, N. M. Kabachnik, and T. Mukoyama, Phys. Rev. A **65**, 062713 (2002).
[36] E. G. Berezhko and N. M. Kabachnik, J. Phys. B: At. Mol. Phys. **10**, 2467 (1977).
[37] H. Yamaoka, M. Oura, K. Takahiro, K. Kawatsura, S. Ito, M. Mizumaki, H. Oohashi, Y. Ito, and T. Mukoyama, J. Phys. B: At. Mol. Opt. Phys. **39**, 2747 (2006).